Pergamon

Int. J. Heat Mass Transfer. Vol. 40, No. 3, pp. 745–756, 1997

0017–9310/97 $15.00+0.00

PII: S0017–9310(96)00091–9

Heat transfer enhancement in laminar flow of viscoelastic fluids through rectangular ducts

PARVIZ PAYVAR

Department of Mechanical Engineering, Northern Illinois University, DeKalb, IL 60115, U.S.A.

(*Received* 13 *October* 1993 *and in final form* 29 *February* 1996)

INTRODUCTION

There are now reliable methods, based on a wealth of experimental and theoretical work, for the accurate prediction of heat transfer in a laminar flow of Newtonian fluids through rectangular ducts. For nonNewtonian fluids this is not true. A number of numerical solutions are available in the literature for flow of power-law fluids through rectangular ducts. The studies by Chandrupatla and Sastri [1], Lawal and Mujumdar [2], and Wibulswas [3] are typical of these solutions which are based on constitutive equations that assume the normal stress coefficients to be zero. The solutions, therefore, predict a completely viscometric flow in the fully developed region. These solutions fail to predict the observed enhancement of heat transfer due to secondary flow as reported by a number of workers. There is considerable evidence now that a realistic prediction of laminar flow heat transfer to viscoelastic fluids must be based on a model more complex than a purely viscous nonNewtonian flow. Green and Rivlin [4], employing a constitutive equation which allowed a nonzero second normal stress coefficient, predicted a secondary flow superimposed on the longitudinal flow in an elliptic duct. Wheeler and Wissler [5], using a similar constitutive equation showed the existence of secondary flows in a square duct. If the walls of the duct are heated, such rheologically induced secondary flows are expected to result in an enhancement of laminar flow heat transfer. Oliver [6] observed an enhancement of heat transfer to aqueous solutions of polyacrylamide and polyethylene of the order of 40% as compared to pure water in flattened coper tubes. Oliver and Karim [7] conducted experimental heat transfer measurements in flattened tubes of aspect ratio 0.18–0.71 and reported up to 45% increase in heat transfer to 250 and 500 wppm solutions of polyacrylamide in water. Mena *et al.* [8] observed a large increase in heat transfer in square ducts in the laminar flow of aqueous solutions of polyacrylamide and assumed secondary flows to be responsible for the enhancement. Kostic [9] and Hartnett and Kostic [10] reported significant enhancement of the Nusselt number with virtually no change in the friction factor in a rectangular duct of aspect ratio 0.5 in the laminar flow of solutions of polyacrylamide in water. Hartnett *et al.* [11] conducted experiments on heat transfer to the laminar flow of Carbopol in a rectangular channel of aspect ratio 0.5. They found that even when the channel is heated only from above, there exists significant enhancement of heat transfer. Clearly, this enhancement cannot be ascribed to free convection effects and must be caused by rheologically induced secondary flows.

A rather comprehensive review of heat transfer to Newtonian and nonNewtonian fluids flowing through rectangular ducts was conducted by Hartnett and Kostic [12]. The need became apparent from this review to explore the suitability of various constitutive models for the prediction of heat transfer to laminar flow of viscoelastic fluids through ducts of noncircular cross-section. In the 1990 Max Jakob Memorial Award Lecture, Hartnett [13] stated several challenges in heat transfer to viscoelastic fluids. Among those challenges is the formulation of predictive methods for heat transfer to the laminar flow of viscoelastic fluids based on a simple model, yet one which captures the physics of the problem.

The objective of the present study is to explore the suitability of constitutive equations which take into account nonzero normal stress coefficients for laminar heat transfer prediction of viscoelastic fluids. In order to have a basis for judging the success of the model, numerical computations are performed for the same fluid, duct cross-sectional geometry, and various dynamical and heat transfer parameters used in the experiments of Hartnett and Kostic [10].

MATHEMATICAL FORMULATION

Figure 1 shows the general flow situation and the coordinate system. Flow enters the duct with a uniform axial velocity w_{in}, pressure p_{in} and temperature T_{in}. The duct is horizontal with the top and bottom surfaces heated in such a way that the heat flux is uniform axially and the temperature of each surface is uniform in the x-direction. The side walls are assumed to be insulated. The fluid is assumed to follow the Criminale, Ericksen, and Filbey (CEF) constitutive equation expressed by Tanner [14] in the form

$$\sigma = -pI+\eta\mathbf{A}_1+v_1(\mathbf{A}_1^2-\tfrac{1}{2}\mathbf{A}_2)+v_2\mathbf{A}_1^2 \qquad (1)$$

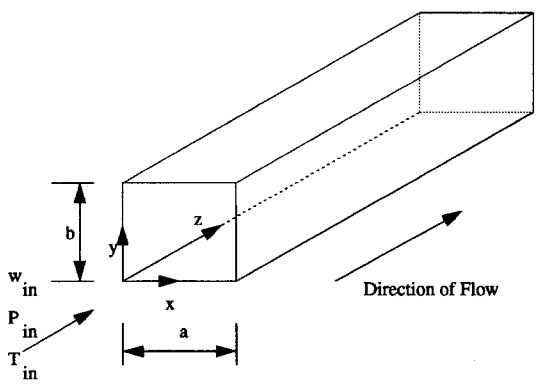

Fig. 1. Geometry and the coordinate system.

NOMENCLATURE

a width of the duct
a^* geometric constant used in Kozicki generalized Reynolds number, equation (23)
$\mathbf{A}_1$ first Rivlin–Ericksen tensor
$\mathbf{A}_2$ second Rivlin-Ericksen tensor
b depth of the duct
b^* geometric constant used in Kozicki generalized Reynolds number, equation (23)
C rheological constant defined by equation (14)
C^* dimensionless second normal stress difference parameter defined by equation (21)
D_h hydraulic diameter
f friction factor defined by equation (37)
F body force in equations (3)–(5)
Gr_q Grashof number defined by equation (20)
Gz Graetz number defined as $Gz = w_{in}D_h^2/\alpha z$
h local mean heat transfer coefficient defined by equation (35)
k thermal conductivity
K rheological constant defined by equation (13)
m rheological property index defined by equation (14)
n rheological property index defined by equation (13)
Nu local mean Nusselt number defined by equation (35)
p local pressure in the cross plane
$\bar{p}$ average pressure driving longitudinal flow
P dimensionless local pressure defined by equation (19)
$\bar{P}$ dimensionless average pressure defined by equation (19)
Pr Prandtl number defined by equation (16)
q_w mean local heat flux at the heated walls
Re axial Reynolds number defined by equation (16)
Re^* Kozicki generalized Reynolds number defined by equation (23)
S cross sectional area of the duct
S_X source term in the x-direction momentum equation (26)
S_Y source term in the y-direction momentum equation (28)
T temperature
T_b bulk temperature defined by equation (36)
T_{in} inlet temperature
u, v, w velocity components
U, V, W dimensionless velocity components
w_{in} inlet fluid velocity
x, y, z Cartesian coordinates as shown in Fig. 1
X, Y, Z dimensionless coordinates defined by equation (17)
Z^* dimensionless axial distance defined by equation (17).

Greek symbols

α thermal diffusivity
α^* aspect ratio of duct cross-section, defined by equation (17)
$\dot{\gamma}$ shear rate magnitude defined by equation (15)
$\dot{\Gamma}$ dimensionless shear rate magnitude defined by equation (22)
η viscosity function
η^* dimensionless viscosity function defined by equation (21)
θ dimensionless temperature defined by equation (20)
ν kinematic viscosity defined by equation (16)
ν_1 first normal stress coefficient as defined by equation (1)
ν_2 second normal stress coefficient as defined by equation (1)
ν_2^* dimensionless second normal stress coefficient defined by equation (21)
ρ fluid density
$\boldsymbol{\sigma}$ stress tensor
σ_{xx} normal stress in the x-direction
σ_{yy} normal stress in the y-direction
$\tau_{xy}, \tau_{xz}, \tau_{yz}$ shear stresses on various planes
ϕ dimensionless temperature defined by equation (20).

Subscripts

b bulk
in inlet
w wall
x denotes direction or differentiation with respect to x
y denotes direction or differentiation with respect to y
z denotes direction or differentiation with respect to z.

with the viscosity function η and the first and second normal stress coefficients ν_1 and ν_2 being functions of shear rate magnitude $\dot{\gamma}$. $\mathbf{A}_1$ and $\mathbf{A}_2$ are the first and second Rivlin–Ericksen tensors. The enhancement of heat transfer in laminar noncircular duct flow due to second normal stress difference is believed to result from secondary flow velocities which are two orders of magnitude smaller than the throughflow velocity. It will be shown below that in this case, the terms involving ν_1 in equation (1) will be much smaller than those involving ν_2, even though existing experimental evidence indicates that ν_1 is one order of magnitude larger than ν_2. The governing equations, neglecting the diffusion terms in the z-direction, are:

continuity

$$\frac{\partial u}{\partial x}+\frac{\partial v}{\partial y}+\frac{\partial w}{\partial z}=0; \tag{2}$$

momentum

$$\rho\left(u\frac{\partial u}{\partial x}+v\frac{\partial u}{\partial y}+w\frac{\partial u}{\partial z}\right)=-\frac{\partial p}{\partial x}+\frac{\partial \sigma_{xx}}{\partial x}+\frac{\partial \tau_{yx}}{\partial y}+F_x \tag{3}$$

$$\rho\left(u\frac{\partial v}{\partial x}+v\frac{\partial v}{\partial y}+w\frac{\partial v}{\partial z}\right)=-\frac{\partial p}{\partial y}+\frac{\partial \tau_{xy}}{\partial x}+\frac{\partial \sigma_{yy}}{\partial y}+F_y \tag{4}$$

$$\rho\left(u\frac{\partial w}{\partial x}+v\frac{\partial w}{\partial y}+w\frac{\partial w}{\partial z}\right)=-\frac{\mathrm{d}\bar{p}}{\mathrm{d}z}+\frac{\partial\tau_{xz}}{\partial x}+\frac{\partial\tau_{yz}}{\partial y}+F_z. \quad (5)$$

Note that pressure terms in the secondary flow plane and the main flow direction have been decoupled. To develop the expressions for the various terms of the stress tensor, two assumptions are made. First, that the secondary flow velocity components u and v and their derivatives are much smaller than the throughflow velocity and its derivatives. Second, that the terms involving the derivatives of the velocity components in the z-direction can be neglected in the expressions for the stress components. Several authors including Tanner [14] have pointed out that such secondary flows are so weak as to be extremely hard to detect by direct measurement. Furthermore, the results of the present study corroborate the soundness of the first assumption. The second assumption is based on the expectation that the hydrodynamic entrance length for the fluids under consideration will be short. Before listing the final expressions for all of the stress components, let us analyze, τ_{xy} and τ_{xz}. With the second assumption, the complete expressions for these components are

$$\tau_{xy}=\eta(u_y+v_x)-\nu_1(u_xu_y+v_xv_y)+\nu_2w_xw_y \quad (6)$$

$$\tau_{xz}=\eta w_x+\nu_1(u_yw_y+\tfrac{1}{2}v_xw_y-\tfrac{3}{2}v_yw_x)+\nu_2(u_yw_y+v_xw_y-2v_yw_x). \quad (7)$$

In equation (6), the term involving the first normal stress coefficient is now seen to be negligible as compared to the term involving the second normal stress coefficient, because of the products of secondary velocity derivatives. In equation (7), the ν_1 term is larger than the ν_2 term based on existing experimental evidence that ν_1 is an order of magnitude larger than ν_2. However, the effect of both terms is negligible as compared to the longitudinal pressure gradient. These conclusions were consistently corroborated by initial exploratory calculations for the highest range of Reynolds numbers considered in this study. Another important result is established by inspection of complete expressions such as equations (6) and (7) for the stress components. That is, if free convection is neglected and ν_2 terms are set equal to zero, the inclusion of the ν_1 terms does not lead to a secondary flow in the fully-developed region. In fact, for this case, regardless of the magnitude of ν_1, the fully-developed solution for the cross plane components is $u=0$ and $v=0$. Analyses similar to those for τ_{xy} and τ_{xz} for the remaining stress tensor components, lead to the following forms used in the final calculations:

$$\sigma_{xx}=2\eta u_x+\nu_2w_x^2 \quad (8)$$

$$\tau_{yx}=\tau_{xy}=\eta(u_y+v_x)+\nu_2w_xw_y \quad (9)$$

$$\sigma_{yy}=2\eta v_y+\nu_2w_y^2 \quad (10)$$

$$\tau_{zx}=\tau_{xz}=\eta w_x \quad (11)$$

$$\tau_{zy}=\tau_{yz}=\eta w_y. \quad (12)$$

Equations (8)–(12) express the hypothesis that the secondary flow is generated substantially by the second normal stress difference and that the effect of the first normal stress difference is negligible, even though the first normal stress coefficient is larger.

The viscometric functions η and ν_2 are assumed to be expressible in power law forms

$$\eta=K\dot{\gamma}^{n-1} \quad (13)$$

$$\nu_2=C\dot{\gamma}^m \quad (14)$$

where $\dot{\gamma}$ is the shear rate magnitude defined as

$$\dot{\gamma}=[2(u_x^2+v_y^2+w_z^2)+(u_y+v_x)^2+(u_z+w_x)^2+(v_z+w_y)^2]^{1/2}. \quad (15)$$

Subject to the assumptions made in this analysis, all terms in equation (15) are negligible except w_x and w_y.

A number of definitions and dimensionless parameters are now introduced in order to present the nondimensional form of the governing equations

$$v=\left[\frac{Ka^{2(1-n)}}{\rho}\right]^{\frac{1}{2-n}}\quad Re=\frac{w_{\mathrm{in}}a}{\nu}\quad Pr=\frac{\nu}{\alpha} \quad (16)$$

$$X=\frac{x}{a}\quad Y=\frac{y}{a}\quad Z=\frac{z}{aRe}\quad Z^*=\frac{z}{D_{\mathrm{h}}}\quad \alpha^*=\frac{b}{a} \quad (17)$$

$$U=\frac{au}{\nu}\quad V=\frac{av}{\nu}\quad W=\frac{w}{w_{\mathrm{in}}} \quad (18)$$

$$P=\frac{a^2(p-p_{\mathrm{in}})}{\rho\nu^2}\quad \bar{P}=\frac{\bar{p}-p_{\mathrm{in}}}{\rho w_{\mathrm{in}}^2} \quad (19)$$

$$\theta=\frac{k(T-T_{\mathrm{in}})}{aq_{\mathrm{w}}}\quad \phi=\frac{k(T-T_{\mathrm{b}})}{aq_{\mathrm{w}}}\quad Gr_q=\frac{g\beta q_{\mathrm{w}}a^4}{k\nu^2} \quad (20)$$

$$\eta^*=\frac{\eta}{\rho\nu}\quad \nu_2^*=\frac{\nu_2}{\rho a^2}\quad C^*=\frac{Cw_{\mathrm{in}}^m}{\rho a^{2+m}} \quad (21)$$

$$\dot{\Gamma}=[2(U_X^2+V_Y^2+W_Z^2)+(U_Y+V_X)^2+(U_Z+ReW_X)^2+(V_Z+ReW_Y)^2]^{1/2} \quad (22)$$

$$Re^*=\frac{\rho w_{\mathrm{in}}^{2-n}D_{\mathrm{h}}^n}{8^{n-1}K\left(b^*+\dfrac{a^*}{n}\right)^n}$$

$$Pe=\frac{w_{\mathrm{in}}D_{\mathrm{h}}}{\alpha}\quad Pr^*=\frac{Pe}{Re^*}. \quad (23)$$

The choice of T_{b} as reference temperature in equation (20) is convenient because it will result in an invariant temperature profile in the fully developed region. With these definitions, the dimensionless governing equations may be expressed as follows:

physical property functions

$$\eta^*=\dot{\Gamma}^{n-1}\quad \nu_2^*=C^*\dot{\Gamma}^m; \quad (24)$$

continuity

$$\frac{\partial U}{\partial X}+\frac{\partial V}{\partial Y}+\frac{\partial W}{\partial Z}=0; \quad (25)$$

momentum

$$U\frac{\partial U}{\partial X}+V\frac{\partial U}{\partial Y}+W\frac{\partial U}{\partial Z}=-\frac{\partial P}{\partial X}+\frac{\partial}{\partial X}\left(2\eta^*\frac{\partial U}{\partial X}\right)+\frac{\partial}{\partial Y}\left(\eta^*\frac{\partial U}{\partial Y}\right)+\frac{\partial}{\partial Y}\left(\eta^*\frac{\partial V}{\partial X}\right)+S_X \quad (26)$$

$$S_X=C^*\frac{\partial}{\partial X}(\dot{\Gamma}^mRe^2W_X^2)+C^*\frac{\partial}{\partial Y}(\dot{\Gamma}^mRe^2W_XW_Y) \quad (27)$$

$$U\frac{\partial V}{\partial X}+V\frac{\partial V}{\partial Y}+W\frac{\partial V}{\partial Z}=-\frac{\partial P}{\partial Y}+\frac{\partial}{\partial X}\left(\eta^*\frac{\partial V}{\partial X}\right)+\frac{\partial}{\partial Y}\left(2\eta^*\frac{\partial V}{\partial Y}\right)+\frac{\partial}{\partial X}\left(\eta^*\frac{\partial U}{\partial Y}\right)+S_Y \quad (28)$$

$$S_Y = C^* \frac{\partial}{\partial X}(\dot{\Gamma}^m Re^2 W_X W_Y) + C^* \frac{\partial}{\partial Y}(\dot{\Gamma}^m Re^2 W_Y^2) + Gr_q \phi \tag{29}$$

$$U\frac{\partial W}{\partial X} + V\frac{\partial W}{\partial Y} + W\frac{\partial W}{\partial Z} = -\frac{d\bar{P}}{dZ} + \frac{\partial}{\partial X}\left(\eta^* \frac{\partial W}{\partial X}\right) + \frac{\partial}{\partial Y}\left(\eta^* \frac{\partial W}{\partial Y}\right); \tag{30}$$

energy

$$U\frac{\partial \theta}{\partial X} + V\frac{\partial \theta}{\partial Y} + W\frac{\partial \theta}{\partial Z} = \frac{1}{Pr}\left(\frac{\partial^2 \theta}{\partial X^2} + \frac{\partial^2 \theta}{\partial Y^2}\right). \tag{31}$$

Note that the expression for S_Y given by equation (29) includes the free convection effect. The parameters of interest in this study are the Reynolds number Re, the Prandtl number Pr, the Grashof number Gr_q, rheological property indices n and m, and the rheological parameter C^*. There is a one to one relationship between the Reynolds numbers Re and the Kozicki Reynolds number Re^* as defined by equation (23), i.e.

$$Re^* = 8^{1-n}\left(b^* + \frac{a^*}{n}\right)^{-n}\left(\frac{D_h}{a}\right)^n Re^{2-n} \tag{32}$$

where a^* and b^* are geometric constants which are given in ref. [12] for rectangular ducts.

The boundary conditions considered in this study are

at $Z = 0$

$$U = 0 \quad V = 0 \quad W = 1 \quad \theta = 1; \tag{33}$$

for $Z > 0$,

$$U = 0 \quad V = 0 \quad W = 0 \tag{34}$$

on all four walls. The thermal boundary condition used for the top and bottom walls is H1, i.e. at these walls the average heat flux is independent of axial location, while at a given axial location each wall is at a peripherally uniform temperature. The two side walls are insulated. The various heat transfer terms are defined as follows:

$$h = \frac{q_w}{T_b - T_w}$$

$$Nu = \frac{hD_h}{k} \tag{35}$$

$$T_b = \frac{\int_s TW\,dS}{\int_s W\,dS} \tag{36}$$

The friction factor f is defined as

$$f = \frac{-\frac{d\bar{p}}{dz}D_h}{\frac{1}{2}\rho w_{in}^2}. \tag{37}$$

THE NUMERICAL SOLUTION METHOD

The numerical solution procedure for three-dimensional parabolic problems was formulated by Patankar and Spalding [15]. The derivation of the discretized equations was performed as in the SIMPLER algorithm of Patankar [16]. The computer program prepared to implement the numerical solution, was written in a general form to allow use of either a uniform or a nonuniform grid. A number of parametric studies were made to decide the number of grid points and the degree of nonuniformity of the grid. Symmetry in the x-direction was assumed. Therefore, the domain of calculations is the left half of the duct cross-section. In the y-direction, symmetry was not imposed in order to allow the existence of free convection effects. Initial calculations were made using 16×20 grids with various degrees of nonuniformity. Graphical outputs from these initial studies, such as contour plots of temperature and secondary flow speed, were used to estimate the extent of regions of sharp velocity and temperature gradients in the vicinity of the walls. Extreme cases such as $Pr^* > 50$ and $Re^* > 1000$ were used to obtain the maximum necessary grid nonuniformity. A sufficient number of grid divisions were then used to capture the sharp variations near all four walls. Based on these initial studies, a nonuniform 18×30 grid was designed for the final calculations. A small forward step size of $\Delta Z = 0.001$ was used near the duct entrance. Further downstream, when the variation of various quantities became smaller, ΔZ was gradually increased. The TDMA algorithm was used to solve the discretized equations by alternately scanning rows and columns. Calculations were continued well into the fully developed region. All calculations were performed with double precision and a sufficient number of iterations were used to reduce all normalized residuals to less than 10^{-6}.

The program was then tested by running a number of cases for which numerical solutions were available in the literature. In particular, heat transfer coefficients for the H1 boundary condition were compared with those calculated by Chandrupatla and Sastri [1] for a power law fluid flowing in a square duct. The fully developed heat transfer coefficients for power law index n ranging from 0.5 to 1 agreed to within 0.1% with those presented by Chandrupatla and Sastri. Figure 2 shows a comparison of the Nusselt numbers calculated in the thermal entrance region with those of ref. [1] for a typical case. The agreement is to within 3% for Graetz numbers less than 100 and improves as fully-developed thermal conditions are reached. Figure 3 shows the effect of mesh size and the degree of nonuniformity on the calculated friction factor for $n = 0.595$ in a duct of cross-sectional aspect ratio 0.5. It is observed that the three sets of results are almost indistinguishable. Figure 4 shows the results of a similar study for the effect of a grid on the calculated Nusselt numbers. The particular case considered was represented by the following values for parameters: $n = 0.595$, $Re^* = 1368$, $Pr^* = 48.10$, $Gr_q = 204.1$ and $v_2^* = -0.317\dot{\Gamma}^{-1.62}$ (run no. 5 in Table 1). Here, it is observed that the values calculated by a coarse uniform grid are up to 17% higher than those calculated by nonuniform grids. The results from the two nonuniform grids, however, agree to within 3%. All final calculations to be presented were obtained by using a 18×30 nonuniform grid in half of the duct cross-section. The reason for the sensitivity of heat transfer quantities to the nature of the grid, is related to the high Prandtl numbers considered. As will be seen in the next section, the high Prandtl numbers coupled with secondary flows, cause sharp temperature gradients near the heated walls. A coarse uniform grid, therefore, is not able to capture the details of the temperature variation in such regions.

For the Newtonian case, the present program was used to calculate friction factors and Nusselt numbers for a rectangular duct, both for the entrance region and for the fully-developed region under a variety of boundary conditions. The results obtained agreed to within 2% with those presented by Shah and London [17]. Based on the above numerical studies, the friction factors and Nusselt numbers calculated are believed to be accurate to within 1 and 3%, respectively.

RESULTS AND DISCUSSION

The objective of the present study is to demonstrate, both qualitatively and quantitatively, that the enhancement of

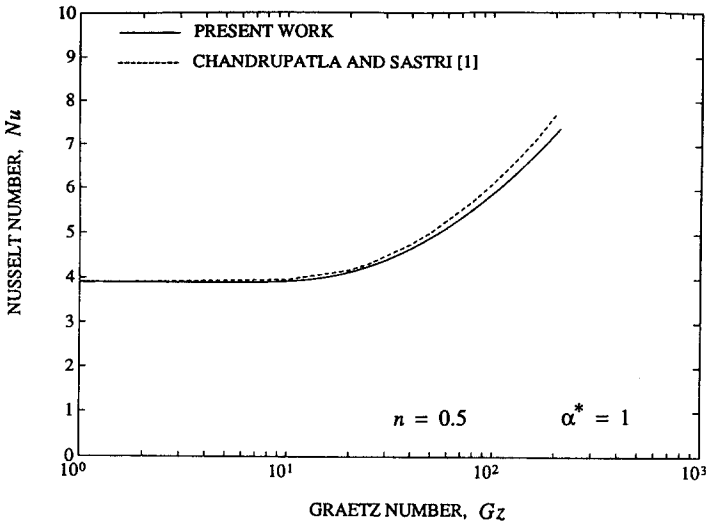

Fig. 2. Comparison of numerically calculated Nusselt numbers for H1 boundary condition.

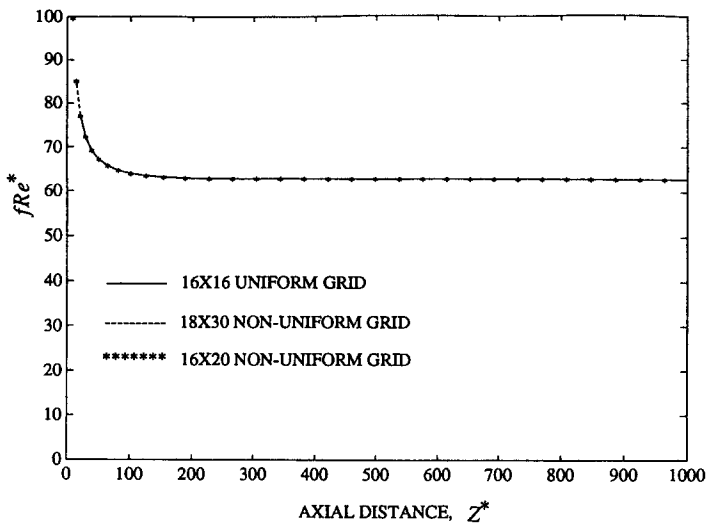

Fig. 3. Effect of mesh refinement and nonuniformity on the calculated friction factors. $Re^* = 1368$, $Pr^* = 48.1$, $n = 0.595$.

laminar heat transfer coefficient in a rectangular duct observed by Kostic [9] and Hartnett and Kostic [10] is due to a secondary flow set up by second normal stress differences. In Table 1, parameters for five experimental runs carried out by Hartnett and Kostic are listed. The test fluid in these experiments was a 1000 wppm solution of polyacrylamide (Separan AP-273) in water. The method of investigation consists of guessing values for C and m in the expression for the second normal stress coefficient v_2 in equation (14), solving the governing equations (24)–(34), and comparing the numerically calculated Nusselt numbers with the experimental values. C and m are changed systematically over a range of values so as to minimize the r.m.s.% difference between the numerical and the experimental results. The suitability of the assumed model is then judged by whether or not a single set of values for C and m would give good agreement with all five runs within the experimental accuracy of the data. Using this method, C and m were found to be -0.0218 ± 0.0022 and -1.62, respectively. The values of C, r.m.s.% deviation, and C^* for each experimental run are given in Table 2. The deviation ranges from 1.56 to 4.37%, well within the estimated experimental uncertainty of about $\pm 5\%$. As values of m other than -1.62 were tried, it was found that a single value for C would not give equally good agreement with all of the experimental runs. For example, Table 2 also shows the values of C corresponding to a value for m of -0.81. It is observed that with this value of m the values of C change from -0.00458 to -0.00072, i.e. by a factor of over 6. Therefore, for $m = -0.81$ it is not possible to find one value for C which would yield uniformly good results at all five Reynolds numbers. Similar conclusions were reached for assumed values of m too different from -1.62. We now turn to studying the detailed results obtained for the optimum values of C and m.

Figure 5 shows the variation of friction factor with longitudinal distance along the duct for $Re^* = 1368$ (run no. 5). The fully developed values of fRe^* with and without the effects of free convection and second normal stress difference are 62.78 and 61.92. These values differ by only 1.38%, corroborating the experimental observation that heat transfer enhancement takes place with practically no change in the friction factor. The hydrodynamic entrance lengths cal-

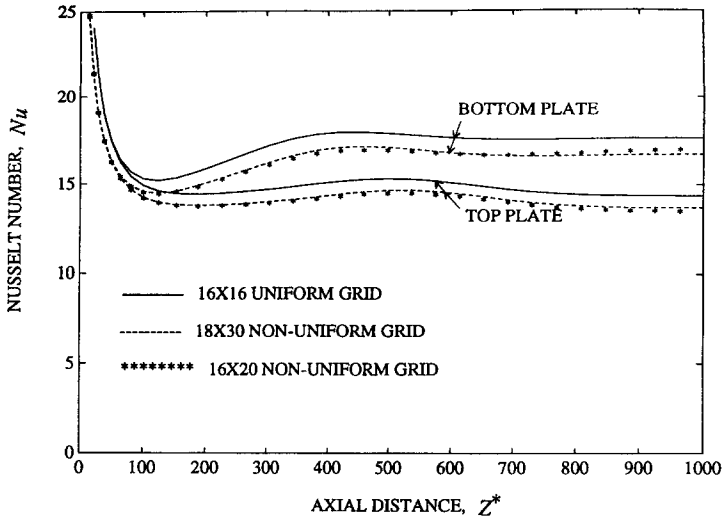

Fig. 4. Effect of mesh refinement and nonuniformity on the calculated Nusselt numbers. $Re^* = 1368$, $Pr^* = 48.1$, $n = 0.595$.

Table 1. Summary of experimental parameters

Run no.	Re^*	Pr^*	Gr_q	n	K	Re	Pr
1	314	79.04	18.1	0.533	0.1236	32.0	1162.7
2	858	55.43	23.1	0.551	0.1053	68.8	1036.9
3	895	54.57	45.5	0.558	0.1009	73.1	1002.0
4	1035	52.01	150.9	0.573	0.0924	86.7	931.0
5	1368	48.10	204.1	0.595	0.0814	117.5	840.0

Table 2. Values of C and m fitted to experimental data

	$m = -1.62$			$m = -0.81$		
Run. no.	C	r.m.s.%	C^*	C	r.m.s.%	C^*
1	−0.024	4.37	−0.230	−0.00458	2.57	−0.00830
2	−0.019	1.56	−0.215			
3	−0.021	1.70	−0.239	−0.00084	1.47	−0.00500
4	−0.024	2.74	−0.300			
5	−0.021	2.35	−0.317	−0.00072	1.53	−0.00497

culated on the basis of reaching to within 5 and 1% of the fully developed value are about 50 and 125 hydraulic diameters. The heated length of the experimental duct was 530 hydraulic diameters. Thus, over the major portion of the heated length, the flow was hydrodynamically fully developed. Similar conclusions were reached for the other four runs.

Figure 6 shows the results of a detailed heat transfer analysis for run no. 5. Two sets of numerically calculated results are shown. The dashed curves show the Nusselt numbers for the top and bottom plate when the free convection effect is included, but v_2 is set to zero. The solid curves are the numerically calculated results with the full model, which allows for both free convection and nonzero v_2. It is observed that free convection alone superimposed on longitudinal flow does not explain the observed enhancement of heat transfer. In fact, the Nusselt numbers for the top and bottom plates are almost the same throughout the experimental heated length of $Z^* = 530$. It is for larger values of Z^* that the free convection effect causes substantial differences between the two plates. The solid curves which show the combined solution due to both free convection and nonzero second normal stress coefficient imposed on longitudinal flow, are quantitatively and qualitatively in agreement with the observed experimental behavior. Free convection effects are now seen to begin at about $Z^* = 100$, while both plates have Nusselt numbers well above that calculated on the basis of pure viscous flow or on the basis of mixed free and forced convection. With the rheologically induced secondary flow, the Nusselt number for the bottom plate reaches to within 1% of its fully developed value at $Z^* = 505$. For the mixed convection solution, the top plate reaches to within 1% of its fully developed value of 12.05 at about $Z^* = 6660$.

Figures 7–9 show the numerical solution for the full model

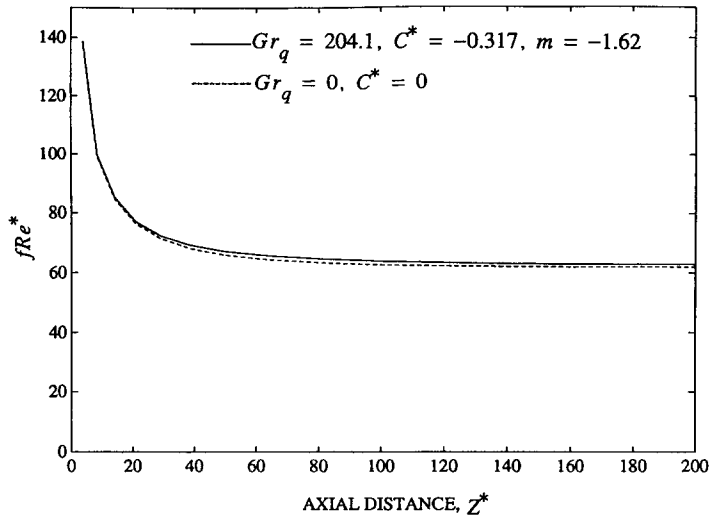

Fig. 5. Effect of secondary flow on the calculated friction factors. $Re^* = 1368$, $Pr^* = 48.1$, $n = 0.595$.

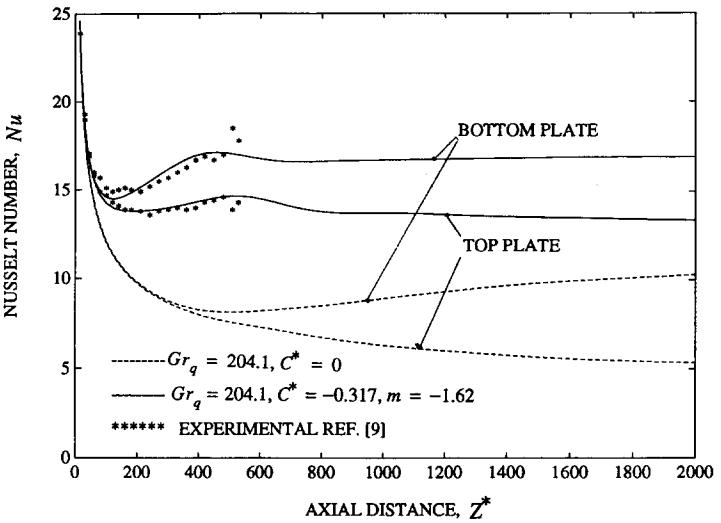

Fig. 6. Comparison of numerical solutions with experimental data of Kostic [9]. $Re^* = 1368$, $Pr^* = 48.1$, $n = 0.595$.

and the purely viscous solution, as well as the experimental data. Data for runs 1–4 was available to this author only in the form of the average of the two plates. In view of even a lesser role for free convection in these runs, this was not an important limitation. It is observed that the model conforms well to the observed magnitude, as well as variation of the Nusselt number. The results in Table 2 show that with $m = -0.81$, it is possible to find a value of C for each run which will result in a numerical solution in agreement with the experimental data. However, as mentioned before, for this value of m, the values of C change by a factor of over 6 in the Reynolds number range considered.

Having gained some confidence that the model represents the physics of this problem well, run no. 5 will now be studied in some more detail. Figure 10(a, b) shows the development of the temperature contours and the secondary flow field from the entrance to the thermally fully developed region. Up to $Z^* = 25$, there is relatively little effect of the secondary flow on the Nusselt number. The thermal boundary layers on both heated walls are almost identical and growing in thickness with axial distance. In this region, the secondary flow is mainly a flow towards the center of the duct as observed in any viscous duct flow. At $Z^* = 24$, two eddies are seen to be evolving. By $Z^* = 180$, the two eddies have assumed their final fully developed form as seen by a comparison to the pattern at $Z^* = 4000$. The effect of secondary flow on the temperature contours starts at about $Z^* = 25$ and continues until full thermal development at about $Z^* = 500$. Figure 10(b) also shows the temperature contours for $Z^* = 4000$, well into the thermally fully-developed region. The slight asymmetry of the temperature contours is due to the effect of free convection. Figure 11 further elucidates the mechanisms involved by comparing streamline patterns and temperature contours for (a) mixed convection only, $v_2 = 0$, (b) no free convection, $v_2 \neq 0$, and (c) combined mixed convection and nonzero v_2. In all three cases the flow is thermally and hydrodynamically fully developed. For mixed convection, the thermal boundary layer on the bottom wall is much

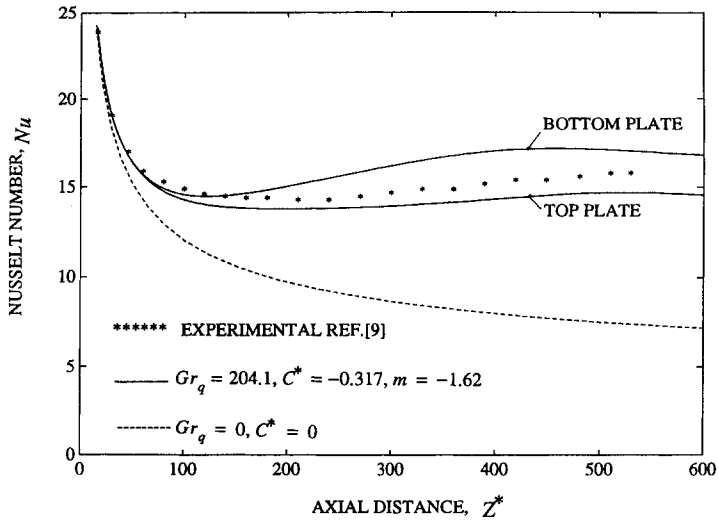

Fig. 7. Comparison of numerical solutions with experimental data of Kostic [9]. $Re^* = 1368$, $Pr^* = 48.1$, $n = 0.595$.

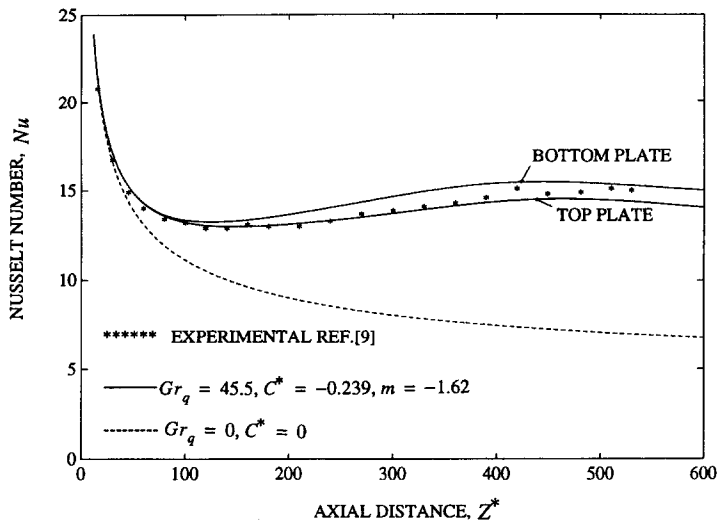

Fig. 8. Comparison of numerical solutions with experimental data of Kostic [9]. $Re^* = 895$, $Pr^* = 54.57$, $n = 0.558$.

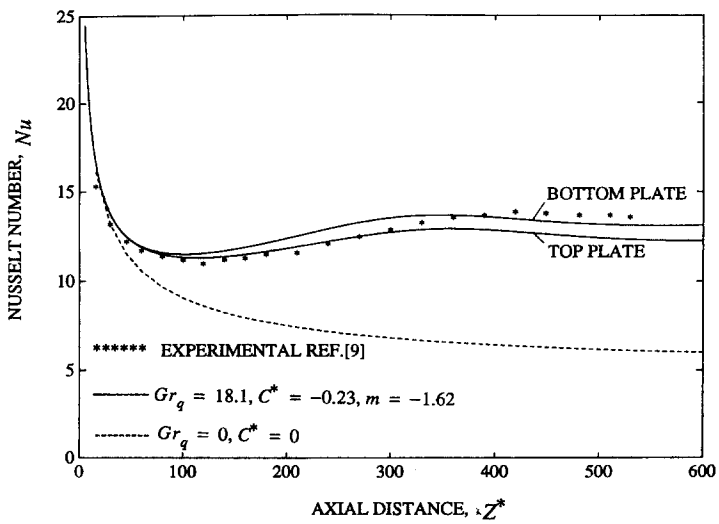

Fig. 9. Comparison of numerical solutions with experimental data of Kostic [9]. $Re^* = 314$, $Pr^* = 79.04$, $n = 0.533$.

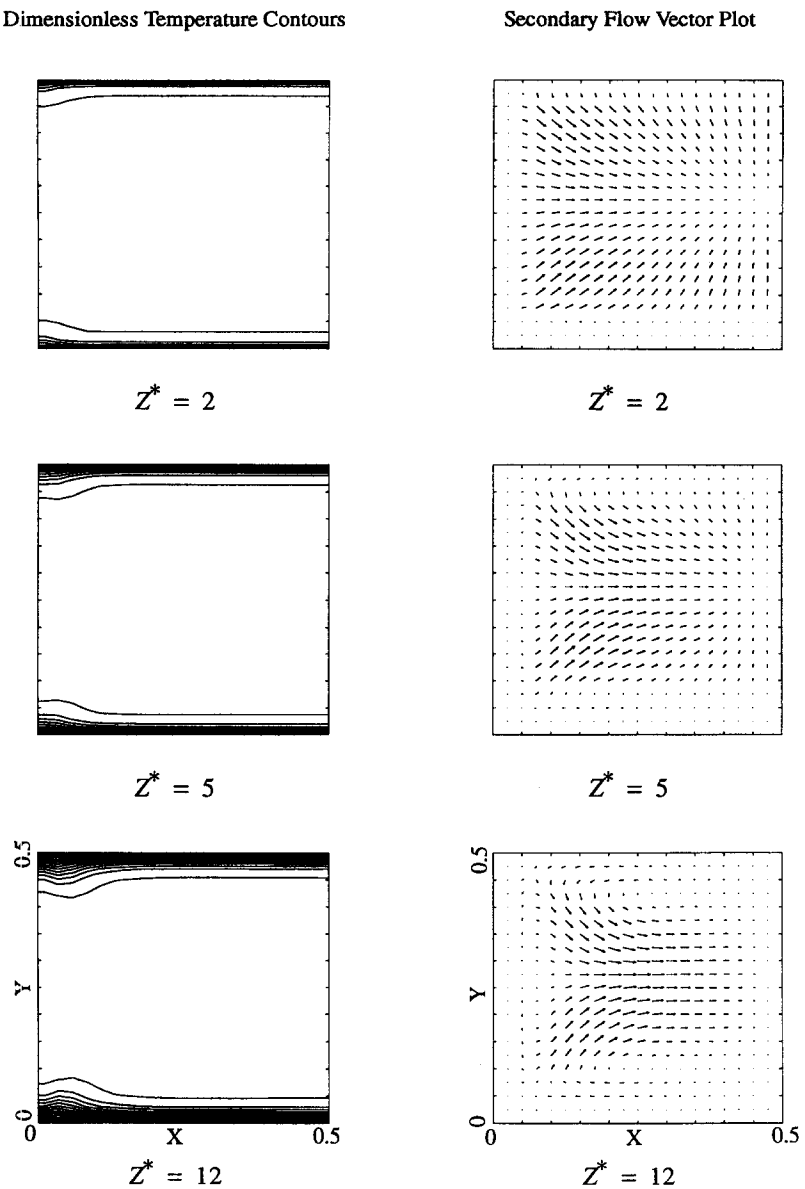

Fig. 10. (a). Temperature contours and secondary flow pattern at various longitudinal locations. $Re^* = 1368$, $Pr^* = 48.1$, $n = 0.595$. (b). Temperature contours and secondary flow pattern at various longitudinal locations. $Re^* = 1368$, $Pr^* = 48.1$, $n = 0.595$.

thinner than that on the top wall. The flow pattern is dominated by a single large eddy occupying the half cross-section. For case (b), there are two main eddies and two smaller eddies occupying the half cross-section. The thermal boundary layers are thin near the center half of each plate and grow rapidly as the end walls are approached. Both flow and temperature patterns are symmetric with respect to the horizontal axis. Finally, case (c) is seen to be quite similar to case (b), except for the slight asymmetry of the flow and temperature pattern due to free convection. For the values of Gr_q and C^* used, clearly the dominant factor determining the nature of the secondary flow is the nonzero second normal stress coefficient.

Figure 12 shows the variation of secondary flow velocity u/w_{in} along the vertical line passing through the center of the eddy for the same three cases (a), (b), and (c). The maximum velocity for case (a) with mixed convection only is about 0.0007, while for the other two cases it is about 0.005. Thus, in all three cases, the secondary flow velocity is very small as compared to the average longitudinal flow velocity, as assumed. The basic assumptions of the model are thus verified. The very small magnitude of the secondary flow velocities makes experimental measurement of these velocities very difficult. In effect, the streamlines have very small curvatures due to the secondary flow and the flow is nearly viscometric.

CONCLUDING REMARKS

The results obtained in the present study demonstrate the suitability of the CEF constitutive equation for the prediction

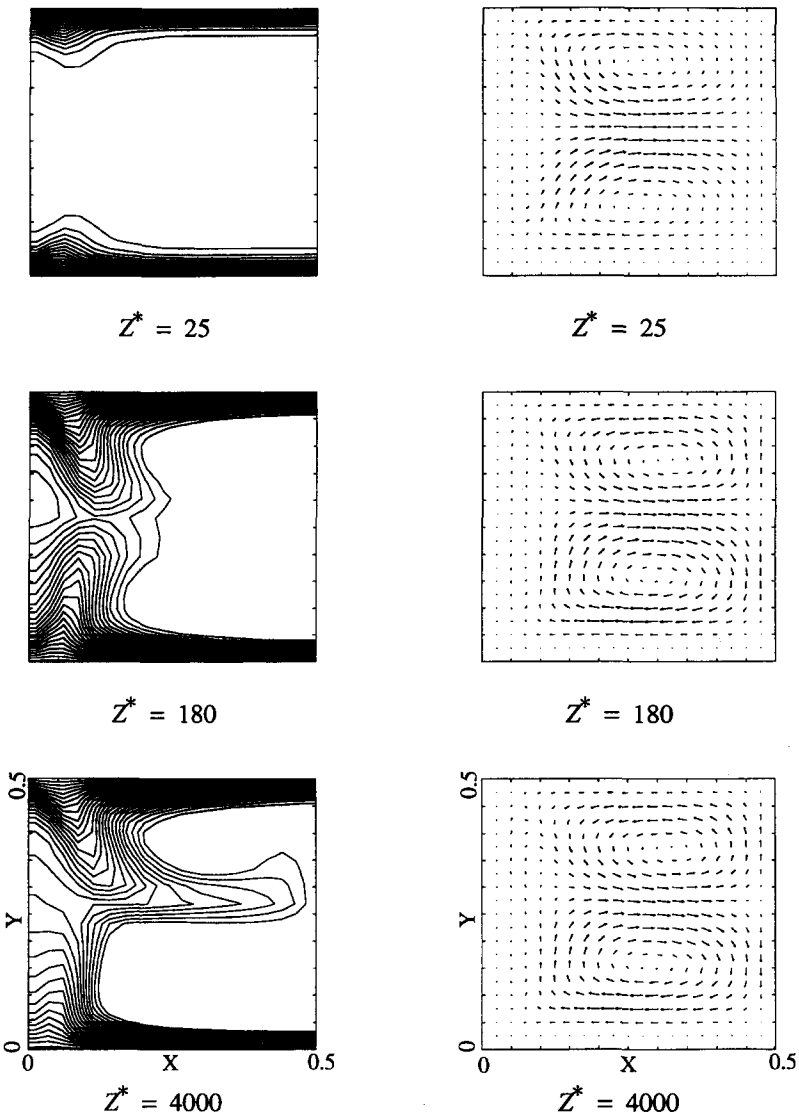

Fig. 10—*continued.*

of heat transfer to the laminar flow of viscoelastic fluids in noncircular ducts. It is demonstrated that the assumed power law form for the second normal stress coefficient with suitable choice of the constants C and m leads to flow and heat transfer results which are in agreement with experimental observation. The study demonstrates the need for a better understanding of the nature of the second normal stress coefficient, as well as development of reliable methods for its measurement. The measurement of the secondary flow velocities remains a challenge due to their small magnitude.

It should be noted from Table 1 that K and n vary somewhat as Re^* changes from 314 to 1368. Most probably, C and m also do change to some extent over the same Reynolds number range and are not strictly constants. Ideally, for both η and v_2, the experimentally determined functions should be used directly in the numerical calculations eliminating the intermediate step of approximating these functions in power law forms.

The numerical method presented in this paper is not limited to power law forms for viscosity and the second normal stress coefficient. In fact, the functional relations established by experimental measurements could be substituted for the power law functions used in this study. In connection with the present study, the numerical work of Gao [18] focusing on the fully developed region should be noted. Also, recent experimental data by Lin *et al.* [19] has confirmed the heat transfer enhancement in laminar flow of CMC solutions. Further work should focus on measurement of second normal stress differences.

Acknowledgements—During the course of the present investigation, the author has benefitted greatly from discussions with Professor Hartnett of the University of Illinois at Chicago and Professor M. Kostic of Northern Illinois University.

Dimensionless Temperature Contours Streamline Pattern

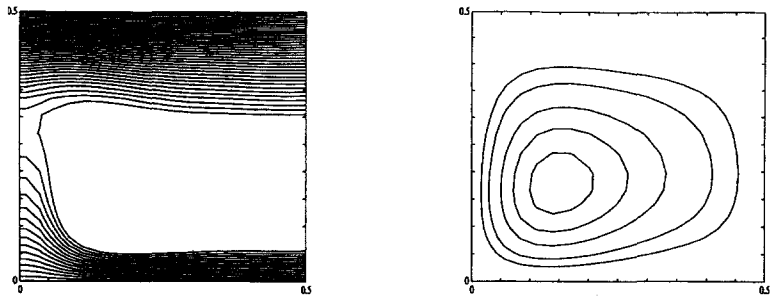

(a) $Gr_q = 204.1, C^* = 0$

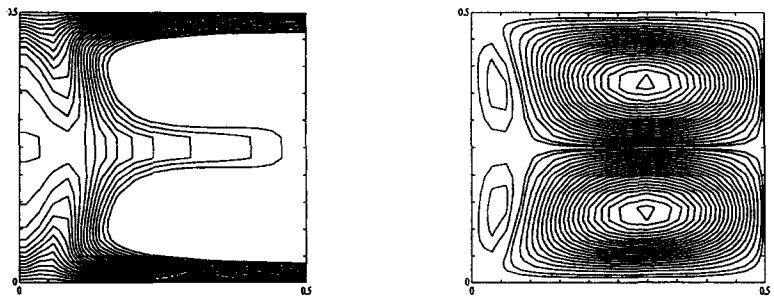

(b) $Gr_q = 0, C^* = -0.317, m = -1.62$

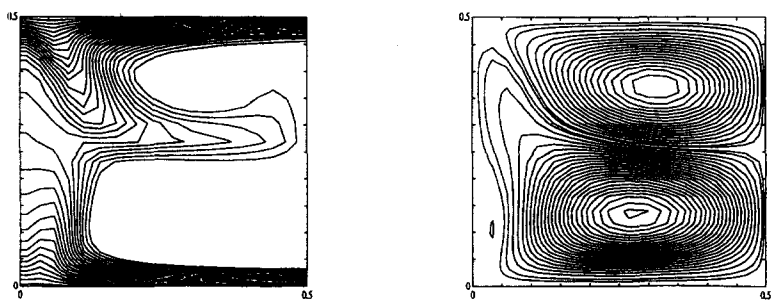

(c) $Gr_q = 204.1, C^* = -0.317, m = -1.62$

Fig. 11. Temperature contours and flow patterns for fully-developed region. $Re^* = 1368$, $Pr^* = 48.1$, $n = 0.595$.

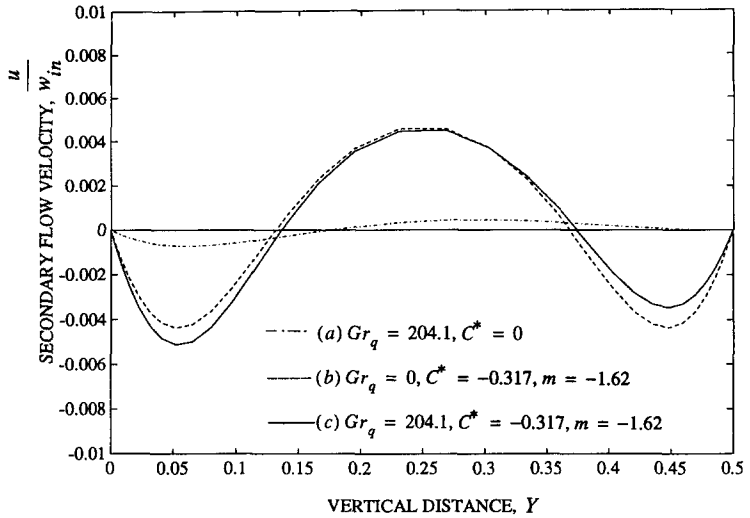

Fig. 12. Magnitude of the secondary flow velocity. $Re^* = 1368$, $Pr^* = 48.1$, $n = 0.595$.

REFERENCES

1. A. R. Chandrupatla and V. M. K. Sastri, Laminar forced convection heat transfer of a non-Newtonian fluid in a square duct, *Int. J. Heat Mass Transfer* **20,** 1315–1323 (1977).
2. A. Lawal and A. S. Mujumdar, Laminar flow and heat transfer in power-law fluids flowing in arbitrary cross-sectional ducts, *Numer. Heat Transfer* **8,** 217 (1985).
3. P. Wibulswas, Laminar-flow heat transfer in non-circular ducts. Ph.D. dissertation, Department of Mechanical Engineering, University of London, London (1966).
4. A. E. Green and R. S. Rivlin, Steady flow of non-Newtonian fluids through tubes, *Q. Appl. Math.* **XIV,** 299–308 (1956).
5. J. A. Wheeler and E. H. Wissler, Steady flow of non-Newtonian fluids in a square duct, *Trans. Soc. Rheol.* **10,** 353–367 (1966).
6. D. R. Oliver, Non-Newtonian heat transfer: an interesting effect observed in non-circular tubes, *Trans. Inst. Chem. Engrs* **47,** T18 (1969).
7. D. R. Oliver and R. B. Karim, Laminar flow non-Newtonian heat transfer in flattened tubes, *Can. J. Chem. Engng* **49,** 236–240 (1971).
8. B. Mena, G. Best, P. Bautista and T. Sanchez, Heat transfer in non-Newtonian flow through pipes, *Rheol. Acta* **17,** 454–457 (1978).
9. M. Kostic, Heat transfer and hydrodynamics of water and viscoelastic fluid flow in a rectangular duct, Ph.D. thesis, University of Illinois at Chicago, IL (1984).
10. J. P. Hartnett and M. Kostic, Heat transfer to viscoelastic fluid in laminar flow through a rectangular channel, *Int. J. Heat Mass Transfer* **28,** 1147–1155 (1985).
11. J. P. Hartnett, C. Xie and T. Zhong, Laminar heat transfer to aqueous carbopol solutions 2:1 rectangular duct, *International Conference on Heat Transfer Energy Conservation*, Shenyang, Peoples Republic of China, October (1988).
12. J. P. Hartnett and M. Kostic, Heat transfer to Newtonian and non-Newtonian fluids in rectangular ducts. In *Advances in Heat Transfer*, Vol. 19, pp. 247–356. Academic Press (1989).
13. J. P. Hartnett, Viscoelastic fluids: a new challenge in heat transfer, *J. Heat Transfer* **114,** 296–303 (1992).
14. R. I. Tanner, *Engineering Rheology*. Oxford Science, Oxford (1985).
15. S. V. Patankar and D. B. Spalding, A calculation procedure for heat, mass, and momentum transfer in three-dimensional parabolic flows, *Int. J. Heat Mass Transfer* **15,** 1787–1806 (1972).
16. S. V. Patankar, *Numerical Heat Transfer and Fluid Flow*. Hemisphere, New York (1980).
17. R. K. Shah and A. L. London, Laminar flow forced convection in ducts. In *Advances in Heat Transfer*, Supplement 1. Academic Press, London (1978).
18. S. Gao, Flow and heat transfer of non-Newtonian fluids in a rectangular duct, Ph.D. thesis, University of Illinois, Chicago, IL (1993).
19. C. Lin, S. Ko and F. K. Tsou, Laminar heat transfer in square duct flow of aqueous CMC solutions, *Int. J. Heat Mass Transfer* **39,** 503–510 (1996).